3D ZEBRA-CROSSING RECONSTRUCTION FROM STEREO RIG IMAGES OF A GROUND-BASED MOBILE MAPPING SYSTEM

[1,2]**B. Soheilian , [1]N. Paparoditis , [1]D. Boldo , [2]J.P. Rudant**

[1]Institut Géographique National / Laboratoire MATIS, 2-4 Ave Pasteur, 94165 Saint-Mandé France
[2]Université de Marne-La-Vallée, Laboratoire Géomatériaux et Géologie de l'Ingénieur, 5 Bd Descartes, 77454 Marne-la-Vallée France
(bahman.soheilian , nicolas.paparoditis , didier.boldo)@ign.fr , jean-paul.rudant@univ-mlv.fr

KEY WORDS: Zebra-crossing detection , Pedestrain crossing , Road-mark , 3D Reconstruction , Mobile mapping , Visual based georeferencing, Edge matching , Robust road plane detection, Close range photogrammetry.

ABSTRACT:

Zebra-crossings are very specific road features that are less generalized when imaged at different scales. We aim to use zebra-crossings as control objects for georeferencing the images provided by a Mobile Mapping System (MMS) using the oriented aerial images of the same area. In this paper, we present a full automatic method for 3D zebra-crossing reconstruction from our MMS calibrated stereo rig. In our image-based georeferencing context, reconstruction accuracy is a priority. The only assumption made is that each zebra-crossing band is supposed to be planar and to have an *a priori* known 3D width. The method consists in reconstructing the 3D edges using a sub-pixel edge matching process by dynamic programming. The detection step is run on all 3D edges around the estimated road plane by looking for parallel segment lines with specific distances. The accurate 3D plane of each band is then estimated from the points belonging to the two previously detected sides. The short sides of each band are detected on the image and are projected onto the 3D plane of the band. Our method is robust and provides promising results. We have a good geometric accuracy.

1 INTRODUCTION

Recently the automation of city modelling from aerial and satellite images has been a prolific field of research. Large scale city modelling from aerial images does not provide accurate facade texture and geometry. For many applications, complementary ground based imagery is necessary. Mobile Mapping Systems (MMS) equipped with cameras and georeferencing devices can provide such data at a low cost. Most of these systems use direct georeferencing devices like GPS/INS, However, in dense urban areas, GPS masks and multi-paths do corrupt measurements quality. Even though INS can help filter GPS errors and interpolate between GPS interruptions, intrinsic drifts of INS will soon accumulate and often lead to absolute metric accuracy, but large scale city modelling implies a positioning accuracy of about $10\ cm$. A solution to cope with this problem is to run a photogrammetric bundle adjustment that integrates measurements from images (tie points) and Ground Control Points (GCP). The main difficulty of this approach is the unavailability of fine GCPs on the vehicle path. Producing a GCP database with traditional surveying techniques (e.g. total station and GPS) would be very expensive and time-consuming.

This is why our general strategy consists in applying the road-marks that have been reconstructed automatically as GCPs from multiple view aerial images of the same area for our bundle adjustment. Indeed, road-marks are very indicative features because of their invariable shapes and very constrained specifications, making their extraction quite an easy pattern recognition problem. Our strategy of road-mark reconstruction form aerial images is detailed in (Tournaire et al., 2006). The same road-marks are automatically reconstructed from images obtained using the ground-based system. Matching terrestrial road-marks with the same road-marks extracted from aerial images will provide an accurate position for the vehicle. The georeferenced images provided in this way can be used for 3D extraction of additional road-marks which can't be reconstructed from aerial images. This can be due to road-mark invisibility or their low size and shape complexity in relation to the low resolution of aerial images. In the present paper, we focus on automatic 3D reconstruction of zebra-crossing from stereopairs obtained from our Stereopolis MMS. Within road-marks, the zebra-crossings are used for georeferencing the terrestrial images because their repetitive and parallel bands make their detection quite easy and they can be found throughout the entire study region. Moreover, other road-marks can be used (arrows, dashed lines, continuous lines). The Stereopolis system (Paparoditis et al., 2005) has been developed at the MATIS laboratory of IGN for automated acquisition and georeferencing of terrestrial images in urban areas. The platform is equipped with three stereoscopic rigs of 4000×4000 CCD cameras. The vertical bases take images of the façades and are used for façade reconstruction (Pénard et al., 2005). The horizontal images (depicted in Figure 1) are used for road reconstruction. The 6 cameras are perfectly synchronized $(10\mu s)$ and provide very high image quality (SNR=300 and 12 bits dynamic range). The intrinsic parameters of each camera and the relative orientations between the cameras are *a priori* estimated using calibration targets with sub-pixel precision and supposed to be rigid. In (Bentrah et al., 2004) the authors present an image-based strategy for relative georeferencing of Stereopolis.

Figure 1: Images provided by horizontal stereo-base of our MMS.

2 OUR STRATEGY

2.1 Previous work

Many authors have investigated automatic road region and road-marks detection from images in the field of robotic and intelli-

gent vehicles. In the GOLD system (Bertozzi and Broggi, 1998), the authors propose a stereovision-based system to be used on a moving vehicle as a navigational aid to increase traffic security. They propose a real-time method for lane detection on a monocular image which benefits from some *a priori* information about the camera position in relation to road and lane size in the image space. The result is a raster detection of lanes with pixel accuracy. In (Se and Brady, 2003) the authors propose a real-time algorithm to detect zebra-crossings and staircases from monocular images. This algorithm is integrated into a system for mobility aid for partially sight-disabled people. The authors propose a method for distinguishing these two features using a slope constraint (horizontal and slanted). In (Utcke, 1997) a method of zebra-crossing detection is proposed which looks for groups of intersecting lines with alternating patterns of light-to-dark and dark-to-light edges. This method makes the assumption that zebra-crossings are planar objects. The percentage of correct detections is about 80%, but the false alert rate reaches 36 out of 163 images.

Work previously mentioned focuses on the detection of road-marks as a pattern recognition problem on a monocular ground-based image. It involves some approximate hypothesis like planar road assumption or known position of camera in relation to the road. In our application the zebra-crossings are used to generate a 3D road-mark database and also for localization of our mobile mapping system. Thus, for our applications, we need a more robust and more exhaustive method. It seems that the intersection and alternating pattern criteria are not sufficient constraints for zebra-crossing detection in urban areas. In fact, many other features on the building facades and on the vehicles can testify to these constraints. So a solution consists in looking for these objects near enough to the correct position (on the road) and in taking into account the particular specifications (given size and shape). Our strategy is to simultaneously process acquired stereopairs to build a 3D description of the scene in which the position and metric specifications of features can be measured. This makes 3D detection more complete and more robust to false alerts.

In a stereo context, some attempts have been made in (Simond and Rives, 2004, Okutomi et al., 2002) for robust road plane estimation. Nevertheless, roads are not always planar. We do not assume that the road surface is perfectly planar in order to provide the most geometrically accurate reconstruction. Our method has to be as robust as possible and exhaustive to handle the geometric anomalies of the zebra-crossing's bands (see Figure 2).

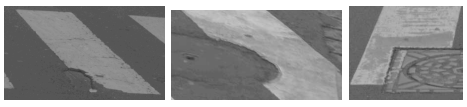

Figure 2: Covered and damaged bands

2.2 Algorithm overview

The first step of our strategy for zebra-crossing reconstruction consists in a 3D reconstruction of edge chains by a dynamic programming optimization approach for matching the edge points globally on the conjugated epipolar lines. The output of this step is a group of 3D edge chains. The second step is to find, within these 3D chains, 3D segment lines that are potential long sides of zebra-crossings. The last step consists in the fine reconstruction of the zebra-crossing shape. Each step of the process presented in Figure 3 will be explained in the next sections.

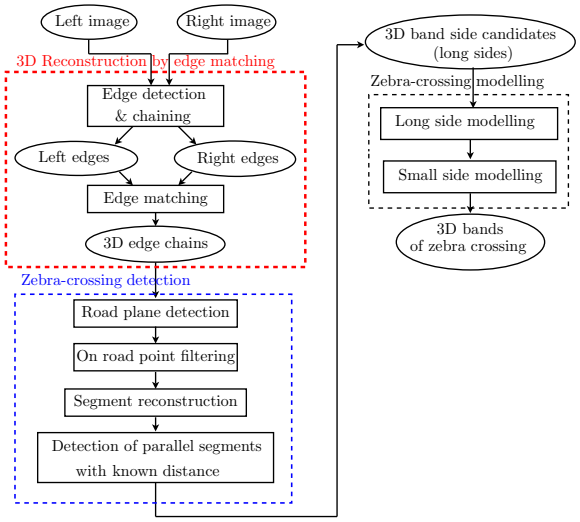

Figure 3: Our zebra-crossing reconstruction strategy

3 3D RECONSTRUCTION BY EDGE MATCHING

In order to reconstruct the zebra-crossing bands, the Canny and Deriche edge detector filter is applied to images of the stereo rig (Deriche, 1987). An edge point matching step is run then to reconstruct the 3D edges. Nevertheless, the stereo base-line is short, thus leading to relatively poor depth estimation. Indeed, our cameras with 29 mm focal length and 9 μm image pixel size, provide a 3 mm across-track and a 4 cm along-track pixel size in object space at a distance of 10 m. In order to decrease the discretization effect due to relatively high along-track pixel size, we need to reach a sub-pixel matching accuracy. This provides more accurate 3D edge chains, which considerably simplifies the pattern recognition step.

In (Han and Park, 2000), the correspondence between two edge chains is estimated from the proportion of edge point correspondences. The efficiency of this algorithm is limited by the effect of fragmentation in the edge chains. In (Serra and Berthod, 1994) the authors propose a dynamic programming approach for sub-pixel edge matching. The matching technique is based on the geometric properties of an edge chain and does not use the radiometric similarity constraints. In (Baillard and Dissard, 2000), an optimized approach is presented for edge point matching with a dynamic programming method along conjugate epipolar lines of aerial images. An initial matching cost function is defined as a combination of intensity and contrast direction similarity. The figural continuity constraint is then implicitly introduced into the final cost function. Minimization is then performed on the total cost along the epipolar line. This approach is very interesting from an optimization point of view and is robust to fragmentation of edge chains.

As seen in Figure 1 our images are not fronto-parallel to the road surface, thus perspective deformations are very strong. To take into account these deformations, an adaptive shape window or image resampling in "vertical" epipolar geometry is applied as described in section 3.2. In addition the very large depth of field in the 3D scene (from 0 to ∞) causes large search space in image. In this case repetitive elements (like zebra-crossings) can be missed in the matching. As we look for the objects on the road surface we limit the search area within a volume around the approximate road surface that we will estimate. This point will be discussed in the following section.

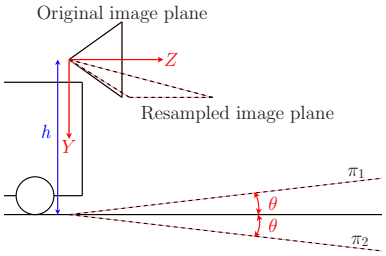

Figure 4: Restriction of search area with road surface

3.1 Search area constraint

As mentioned before in our terrestrial imaging system, the very large depth of field and perspective effects are the main difficulties in the matching process. These two problems can partially solved by limiting the search area around each principal plane of the scene (facades and road) followed by a perspective rectification of each image.We will thus define our search area around the approximate road surface to match the road features. This is achieved using the approximate pose of the cameras in relation to the road surface. As seen in Figure 4, the stereo rig is mounted horizontally on the vehicle at a height h from road surface. The Y axis is supposed to be perpendicular to the road surface with a tolerance θ. This θ depends on vehicle deviation in relation to the road. Thus, the search interval is reduced to the volume between two planes (π_1 and π_2). Parameter θ can be optimally chosen for each exposure by estimating the camera deviation in relation to the 3D architectural scene via vanishing point detection as done in (Cipolla et al., 1999); or, it can be easily chosen comparatively greater than the maximum deviation of vehicles relative to the road (θ_{max}).

3.2 Similarity constraint

In (Baillard and Dissard, 2000) the similarity measurement between two edge points is calculated as a combination of the differences in grey level on each side of the edge point and the direction of contrast. In (Han and Park, 2000), the similarity function is a classical normalized correlation coefficient calculated in a $(2n+1 \times 2n+1)$ window.

As explained in the previous section, the search area is limited to a volume around the road surface. To avoid false matches due to road obstacles (e.g. vehicles and pedestrians), a "road plane" adaptive shape correlation window of large size (11×11) has been used. With this strategy the aim is to implicitly filter most obstacles in the reconstruction step. This process removes many false matches. The reconstructed 3D edge chain has adequate quality in the centre of the images, but edge chains are fragmented near the image corners. This is due to important perspective deformation between the two images that makes an important difference in segment direction from one image to another. Figure 5(a) shows the edge chain matching issue in a direction parallel to the epipolar line. The matching result as seen in figure 5(b) causes the fragmented chains. This fragmentation effect can be removed by chaining isolated pixels but the 3D reconstructed chain will be of poor quality because of interpolation.

To resolve this issue, we prefer resampling the images in an epipolar geometry where the image's normal vector is set approximately parallel to the terrain Z axis (see figure 6). While rectifying images, we take into account the distortions to build "distortion-free" images. From now these rectified images will be used whenever image information is needed.

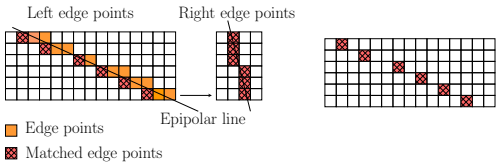

(a) The edge chains in stereo images (b) Matching result

Figure 5: Matching edges with perspective deformation

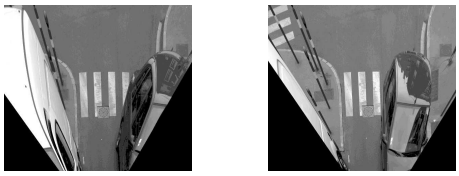

Figure 6: The resampled images used for reconstruction

3.3 Edge matching results

The optimized matching process by dynamic programming provides a disparity map with pixelar matching quality. As discussed before, because of very low B/H a sub-pixel matching quality is needed. This is achieved by post processing step involving sub-pixel edge re-localization along the gradient direction in each image as in (Devernay, 1995). The sub-pixel matching estimation is then computed at the intersection of the sub-pixel epipolar line and subpixel edge chains. Figure 7 shows the 3D sub-pixel reconstructed edges.

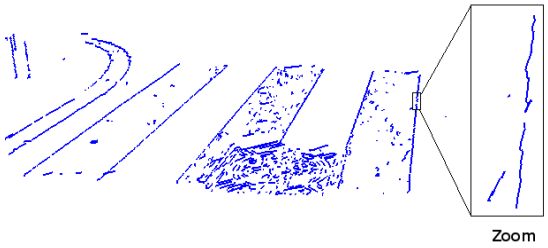

Figure 7: Reconstructed 3D edges. $\theta = 4°$

4 ZEBRA CROSSING DETECTION

As explained in the previous section edge chains are reconstructed in 3D. The reconstruction is precise but 3D edge chains are very low-level primitives. As shown in Figure 7 most of the edges we are interested in are reconstructed as well as many others including false matches. Figure 2 shows that zebra-crossing bands are sometimes damaged and do not completely form straight lines. So, we need a robust detection method to filter out the non interesting features and to produce higher level features like 3D segment lines from the 3D edge chains. The principal goal of this detection step is to get hypothetical zebra-crossing band candidates. The detection process takes advantage of the given specifications of zebra-crossings as defined in section 4.1. The detection method is performed on all of the 3D chains around the road plane. This plane is detected automatically as will be explained in section 4.2. The final segment line candidate are computed without any planar hypotheses assumption using initial 3D coordinates. The detection method is discussed in section 4.3.

4.1 Zebra-crossing specifications

In France, the zebra-crossings are painted on the roads accordintg to strict specifications (Transport Ministry and Interior Ministry, 1988). A zebra's band in urban areas is a parallelogram of $50cm$ width and $2.5m$ minimum length . However, accurate length and exact shape (angle between long and short sides) of the band are unknowns. Each band is supposed to be planar but due to transversal road curvature, the zebra as a whole is not a planar feature.

4.2 Principal plane detection

Here the goal is to detect the features that lie on the road surface. We assume that in the first approximation, the road surface can be represented as a plane. Indeed, a large number of reconstructed chains are near enough to an average plane, however, some outliers are mixed into the data. A RANSAC algorithm (Fischler and Bolles, 1981) is used to find a robust 3D plane (with a tolerance of 20 cm). To refine this estimation, a least squares technique is then carried out on the remaining samples (close to the 3D plane). The features with distances greater than 20 cm from the computed plane are filtered out.

4.3 Detection of zebra-crossing long sides

In the next step the remaining 3D edges are projected onto the estimated road plane to transform the detection problem from 3D to 2D. Nevertheless, let us point out that true 3D coordinates for each detected segment without any planar assumptions will be available for the final reconstruction.

As can be seen in Figure 7, extracted edge chains suffer from fragmentation due to local texture. To generate initial line segments, a classical algorithm (Douglas and Peucker, 1973) is used to polygonalize the edge chains. In order to refine the estimation of each side of the polygon, a 2D line segment regression is performed on all the edge points that are contributed using the approach presented in (Deriche et al., 1992).

As seen in figure 8(a) an accumulation space is defined perpendicular to the principal direction of the line segment set. The principal direction is the most frequently occurring direction within the set. Each line segment votes in cells in which it projects along the principal direction. The score is proportional to the part of the segment, which project in each cell. Accumulation cell's size is proportional to the reconstruction precision and to the chosen tolerance for the detection step. The peaks in the accumulation diagram correspond to the existence of straight lines in the principal direction. In practice a hysteresis thresholding is carried out in this diagram to extract the connex components. The thresholds are defined regarding the minimum band length L (20% and 5% of minimum band length it means 20% and 5% of $2,5\ m$). This hysteresis thresholding robustifies the method to discretization effects in accumulation space. For each component we look for its neighbouring component at a distance equivalent to the specified band width. The component is filtered, if no other component is available. For each remaining component, all segment lines that have contributed to the component, will be candidates for grouping in order to generate the longer line segments. Usually not all the segments of one component are to be regrouped. For example in figure 8(a), some segments of manhole-cover contribute to the band segments to a connex component. Therefore, the candidates for grouping are generated by measuring the difference of orientation and closeness between segments. A globally more favorable grouping is then chosen as in the approach presented in (Jang and Hong, 2002). In practice, the grouping process is performed in two steps. Considering that orientation uncertainty is higher for short segments, first a grouping is made with a fine threshold for closeness and a coarse one for orientation difference to favour the regrouping of short and close segments. Too little segments are then filtered out. The reconstructed segment results in our running example are shown in Figure 8(b). The first step provides the longer segment lines with lower uncertainty of orientation and the second one is made with a fine threshold of orientation and coarse threshold of closeness (see Figure 8(c)). The second step gathers broken segment lines (break due to a damaged zebra-crossing band or an occlusion). The output of our grouping step is a global 2D segment with information from the initial 3D segments contained in the grouping. Knowing the 3D coordinates of each contributed line segment, a final 3D line segment is estimated by a 3D regression on all the 3D segments that have been contributed. In an ideal case, if all edge chains that go into the reconstruction of a side of the zebra-crossing are detected, a complete 3D segment line (on the entire length of the band side) can be estimated. In this case, the segments that are smaller than the minimum specified length of band can be filtered-out. Sometimes, due to the road curvature along a band side such a segment line can't be reconstructed. So, the line segment candidates are filtered with a lower threshold. The longer the line segment candidate is, the more precise the reconstruction is. In section 6, the effect of this parameter on the results will be discussed.

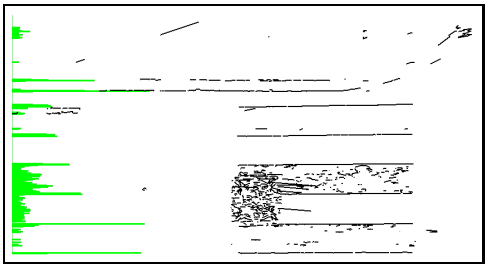

(a) Initial chains and accumulation in grey on the left

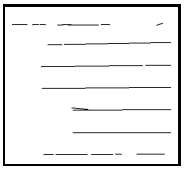

(b) After first filtering and regrouping

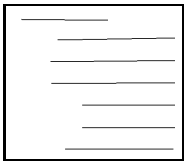

(c) After second regrouping

Figure 8: Parallel segment detection

5 ZEBRA-CROSSING MODELING

The segment hypotheses for long sides of a band are projected into the image space. For each segment a measure of gradient direction is calculated using the images of gradient in two directions (x and y). Then, we look iteratively for pairs of line segments with inverse gradient direction and with a distance equivalent to band width. Figure 9 shows how the gradient direction is used to generate the bands by grouping two segment candidates. Such pairs of segments form a band and a 3D plane is estimated using these segments. This plane will be the final plane of the band. The band is then modelled as a quasi-parallelogram. The band vertices are defined as the intersection of the long sides and the transversal sides in image space. These vertices are then projected onto the band's 3D plane. The plane of each band is calculated independently and the zebra-crossing is not constrained to be planar. The following section explains how the transversal bands are modelled.

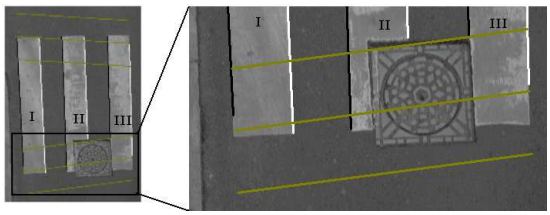

Figure 9: Constitution of the bands. The light lines correspond to the search space for transversal side detection

5.1 Transversal side band modelling

As seen in igure 9, the estimated long sides of the band, are tangent to the true position of the band but the extremity of these segments are not correctly positioned and a little part of the side is missing (see band I in figure 9). In the presence of covering objects like stains or manhole-covers the long sides are not complete (see band II in igure 9). In addition, the accurate angle between two sides of a zebra-crossing band is unknown. This is why only with the long sides the parallelogram modelling is not possible. So, we aim at detecting the transversal sides and to calculate the vertices of the parallelogram as the intersection of the long sides and transversal sides. According to section 4.1, let us suppose that the transversal sides are quasi-parallel and of inverse gradient directions. Search space is defined for side detection around the extremities of the bands. For each band, a pair of quasi-parallel sides is detected optimally in the search area by maximizing a gradient-based score. The search space is defined around an approximate transversal side in 3D. The approximate transversal side is estimated on the zebra-crossing in it's whole by a 3D regression on the extremities of the longer sides (up to 80% of the maximum length). A sufficiently large neighbourhood around this band ($40\ cm$ on each side) is accepted. The limits of the search space are then projected onto the image (as seen in Figure 9). The intersection of the two long sides of a band and the previously defined area constitutes a search area on each side of a band. A Hough transformation is performed on the edges within the search area to detect the lines with orientation near the approximate transversal side orientation (up to $20°$). The set of a local maximum with a Hough score higher than 80%

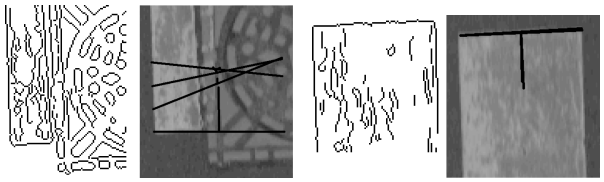

(a) Downward search area with 4 hypotheses (b) Upward search area with 2 hypotheses

Figure 10: Edge points in the search area of band II

of the highest maximum are accepted as side candidates (see Figure 10).We look for the best pair of quasi-parallel segment lines with maximum contrast as the final transversal sides. In order to do this, a gradient vector ($\vec{\Gamma}$) is calculated for each line (see equation 1). Figure 10 shows the set of accepted segment lines and the corresponding vector $\vec{\Gamma}$. A global $Score$ is then defined according to equation 2 for each pair of hypotheses for a band.

$$\vec{\Gamma_t} = (\sum_{s \in t} G_x(s), \sum_{s \in t} G_y(s)) \quad (1)$$

t : Estimated hough line , s : Point in t,
$G_{x\ or\ y}$: Deriche gradient in x or y directions. All other gradient operators can be used.

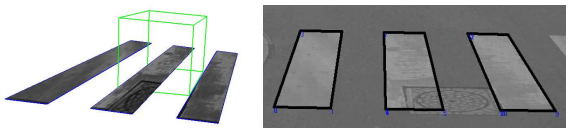

(a) 3D textured reconstructed bands (b) Image projection of reconstructed bands

Figure 11: Zebra-crossing modeling results

$$Score_{t \in U, l \in V} = \left\| \vec{\Gamma_t} \right\| + \left\| \vec{\Gamma_l} \right\| \quad (2)$$

t, l : Candidates for the upward and downward transversal bands, U, V : Set of estimated line with Hough for the downward , the upward of a band.

Secondary higher peaks of $Score$ (up to 80% of maximum $Score$) are accepted. In order to find the best pair with inverse gradient direction criteria the final two transversal sides (i, j) are found by equation 3.

$$(i, j) = \underset{t \in U, l \in V}{\operatorname{argmin}} (\vec{\Gamma_t}.\vec{\Gamma_l}) \quad (3)$$

The 4 vertices of the band are then calculated by intersecting the long sides and the transversal sides. These vertices are then projected onto the previously calculated 3D plane of the band. Carrying out the same procedure for each detected band provides the 3D zebra-crossing model. Each band is reconstructed independently. We do not assume a planar model for zebra-crossing. The transversal curvature of the road can thus be reconstructed precisely. Figure 11 shows reconstruction results on our running example.

6 RESULTS AND EVALUATIONS

In order to evaluate the robustness of our algorithm it has been applied to 15 stereopairs of images obtained in a test survey in the city centre of Amiens in France. Only the bands of quasi-parallelogram form are taken into account in our evaluation. These bands could be partially occluded or damaged (see Figure 2),but the bands with any transversal side occluded are not taken into account in evaluation. Our sample comprises a set of 82 bands of different zebra-crossings. The test is performed first with $L_{min} = 1\ m$ in the detection step (see section 4.3) to ensure good reconstruction. We then measure the number of detected bands and also the number of good reconstructions. The bands are considered correctly reconstructed if the projections of its sides in stereo pair images are qualitatively as close as 1 pixel to the images band sides. We prefer to evaluate the band with its sides rather than its vertices because the vertices in reality are damaged and not clearly defined. As RMS accuracy normally depends on the resolution of the image, it is provided in pixels in the evaluation. As seen in Table 1, the rate of detection is about 92% with 92% of good reconstruction within the detected ones. The detection rate can be increased with $L_{min} = 0.2\ m$ to 97% with 89% of good reconstructions. In the two cases we had only 1 false alarm that could be filtered by taking into account the minimum and maximum distances criteria between the bands.

The RMS accuracy depends on the depth and orientation of the zebra-crossing in relation to the stereobase, Therefore $L_{min} = 0.2\ m$ is applied to take into account the smaller and more uncertain segment lines as well. Figure 12 shows the performance of our reconstruction algorithm for a very unfavourable stereopair. The zebra-crossing is at a distance of $20\ m$ from our $1\ m$

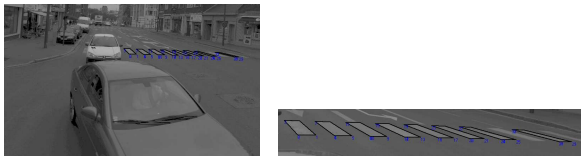

(a) Relative position to stereobase

(b) 8 bands out of 10 are detected and 6 are correctly reconstructed.

Figure 12: Reconstructed zebra-crossing with $B/H = 0.05$.

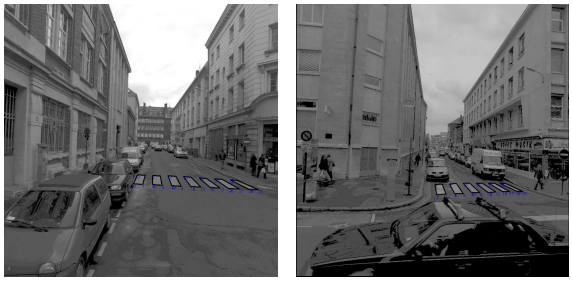

(a) 7 bands out of 7 are detected and correctly reconstructed

(b) 6 bands out of 6 are detected. 1 band is not correctly reconstructed due to non-flat band

Figure 13: Image projection of 3D reconstructed zebra-crossing

stereobase. The right extremity of the zebra-crossing is situated near the corners of the stereopair, so the angle of intersection in the reconstruction step is very small. In our specific mobile mapping application, the high frequency of image acquisition provides many images from one zebra-crossing; therefore, in order to be more precise in the reconstruction, we use only the nearest stereo-pair with $L_{min} = 1m$. So, if we use only the nearest stereopairs to zebra-crossings the detection rate is 100%, 90% of detected bands are correctly reconstructed. Figure 13 shows the image projection of a reconstructed zebra-crossing with $L_{min} = 1\ m$.

L_{min}	Visible band	Detected	Correct reconstruction
$1\ m$	83	76 (92%)	70 (92%)
$0.2\ m$	83	81 (97%)	72 (89%)

Table 1: Zebra-crossing detection and reconstruction results.

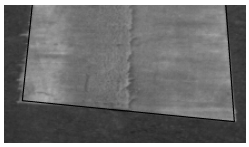

Figure 14: Projection of reconstructed band in image

In order to compare our 3D reconstructed model with the terrain reality, 3D measurements are performed by surveying techniques with millimetre precision on a zebra-crossing containing 4 bands. A stereopair is used to reconstruct the same zebra-crossing. A rigid transformation is then applied to place these two models (reconstructed and terrain reality) in the same coordinate system. The difference between two models is then measured as the average distance between the 4 points of each band in 2 models. We have found a maximum distance of $4\ cm$ with an RMS of $2\ cm$. $2\ cm$ of difference is acceptable for our reconstruction due to definition limit for a real zebra-crossing. As seen in figure 14, the band corners of a real zebra-crossing are not well defined due to local texture.

7 CONCLUSION AND FUTURE WORK

We have presented an original algorithm for 3D zebra-crossing reconstruction from rigid stereopairs in urban areas. The evaluation revealed robustness and completeness of our algorithm, to different sizes, shapes, orientations and positions of zebra-crossings in the images. This algorithm is also quite generic. Indeed it can be applied very easily to any other 3D planar parallelogram. We will also generalize our approach to deal with all other road-marks in order to build a complete road-mark GIS.

REFERENCES

Baillard, C. and Dissard, O., 2000. A stereo matching algorithm for urban digital elevation models. ASPRS journal of Photogrammetric Engineering and Remote Sensing 66(9), pp. 1119–1128.

Bentrah, O., Paparoditis, N., and Pierrot-Deseilligny, M., 2004. Stereopolis : an image based urban envi-ronments modeling system. In: the 4th International symposium on Mobile Mapping Technology, China.

Bertozzi, M. and Broggi, A., 1998. GOLD: A parallel real-time stereo vision system for generic obstacle and lane detection. IEEE Tr. Im. Proc. 7(1), pp. 62–81.

Cipolla, R., Drummond, T. and Robertson, D., 1999. Camera calibration from vanishing points in images of architectural scenes. In: BMVC.

Deriche, R., 1987. Using canny's criteria to derive a recursively implemented optimal edge detector. The International Journal of Computer Vision 1(2), pp. 167–187.

Deriche, R., Vaillant, R. and Faugeras, O., 1992. From Noisy Edges Points to 3D Reconstruction of a Scene : A Robust Approach and Its Uncertainty Analysis. Vol. 2, World Scientific, pp. 71–79. Series in Machine Perception and Artificial Intelligence.

Devernay, F., 1995. A non-maxima suppression method for edge detection with sub-pixel accuracy. Technical Report RR-2724, INRIA.

Douglas, D. H. and Peucker, T. K., 1973. Algorithms for the reduction of the number of points required to represent a digitized line or its caricature. The Canadian Cartographer 10(2), pp. 112–122.

Fischler, M. A. and Bolles, R. C., 1981. Random sample consensus: A paradigm for model fitting with applications to image analysis and automated cartography. Communications of the ACM 24(6), pp. 381–395.

Han, J. H. and Park, J.-S., 2000. Contour matching using epipolar geometry. IEEE Transactions on Pattern Analysis and Machine Intelligence 22(4), pp. 358–370.

Jang, J.-H. and Hong, K.-S., 2002. Fast line segment grouping method for finding globally more favorable line segments. Pattern Recognition 35(10), pp. 2235–2247.

Okutomi, M., Nakano, K., Maruyama, J. and Hara, T., 2002. Robust estimation of planar regions for visual navigation using sequential stereo images. In: IEEE ICRA, pp. 3321–3327.

Paparoditis, N., Bentrah, O., Pénard, L., Tournaire, O., Soheilian, B. and Deveau, M., 2005. Automatic 3D recording and modeling of large scale cities : the ARCHIPOLIS project. In: Recording , Modeling and visualisation of cultural heritage, ASCONA.

Pénard, L., Paparoditis, N. and Pierrot-Deseilligny, M., 2005. 3D building facade reconstruction under mesh form from multiple wide angle views. In: Proceedings of the ISPRS Commission V/4 Workshop 3D-ARCHE, Vol. XXXVI, Part 5/W17, Italy.

Se, S. and Brady, M., 2003. Road feature detection and estimation. Mach. Vision Appl. 14(3), pp. 157–165.

Serra, B. and Berthod, M., 1994. Subpixel Contour Matching Using Continuous Dynamic Programming. In: ICVPR, Seattle, pp. 202–207.

Simond, N. and Rives, P., 2004. Détection robuste du plan de la route en milieu urbain. In: RFIA.

Tournaire, O., Paparoditis, N., Jung, F. and Cervelle, B., 2006. 3D roadmarks reconstruction from multiple calibrated aerial images. In: Proceedings of the ISPRS Commission III PCV, Germany.

Transport Ministry and Interior Ministry, 1988. Instruction interministerielle sur la signalisation routiere : septième partie partie 1. Technical report.

Utcke, S., 1997. Grouping based on projective geometry constraints and uncertainty. Internal report, Technische Informatik I, TU-HH, Hamburger Schloβstraβe 20 D-21071 Hamburg Germany.